Monolithic Integration of Nanoscale Solid Oxide Fuel Cell Membranes onto Polymer Scaffolds through Stress Control

Kian Kerman,* Quentin Van Overmeere,† Michael Karpelson, Robert J. Wood, and Shriram Ramanathan

School of Engineering and Applied Sciences, Harvard University, Cambridge, Massachusetts 02138, United States. †On leave from the Institute of Mechanics, Materials and Civil Engineering, Université catholique de Louvain, B-1348 Louvain-la-Neuve, Belgium.

ABSTRACT Ultrathin fast-ion conducting oxide membranes are of broad interest to a range of energy conversion technologies. We demonstrate a low-temperature (<30 °C) process for controlling internal stress in an archetypal fast-ion conductor, crystalline Y_2O_3-doped ZrO_2 (YDZ), which allows us to form stable suspended nanomembranes akin to those fabricated at high temperature (>550 °C). Such a low-temperature synthesis method then enables us to monolithically integrate the suspended oxide-ion conducting membranes onto polyimide (Kapton by DuPont), a polymer with vastly different physical properties than that of a ceramic. Integrated functional heterostructure solid oxide fuel cells operable below the glass transition temperature of the polymer are demonstrated. Our results describe a mechanistic low-temperature processing route for forming stable multifunctional membrane structures, applicable to the realization of various energy conversion and sensing devices and structural skins for miniature autonomous systems.

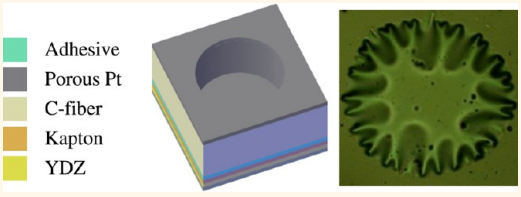

KEYWORDS: thin film solid oxide fuel cells · membranes · structural power source · room temperature processing · thin film stress · quasi-two-dimensional

High-temperature processing is often required to fabricate crystalline oxide thin films, which may hinder application in a variety of heterogeneously integrated devices, such as on low melting temperature polymeric substrates. Concerns such as material degradation, interfacial reactions, or interdiffusion limit the choice of compatible substrates for oxide film growth or device integration. There has been a significant effort to utilize low-temperature processing for thin film electronics including combustion and sol–gel processes.[1,2] However, only partial crystallization is exhibited at low temperature,[1] and amorphous films require high-temperature annealing.[2] Postprocessing crystallization and subsequent volume change can catastrophically affect the mechanical integrity of free-standing membrane structures.[3] Ultrathin oxide membranes with low ionic resistance are of great interest for reduced temperature solid oxide fuel cells (SOFCs) for mobile energy,[4,5] gas separation,[6] elucidating mechanical–chemical interplay,[7] and low-power sensors where functionality can be realized at sub-400 °C. Understanding the interplay between materials synthesis, mechanics, and functionality of ultrathin oxide membranes is a substantial challenge. Internal stress (σ_0) in the oxide film is a crucial component for the design of self-supported membranes.[8−10] In polycrystalline thin films, σ_0 is related to many factors including film thickness, deposition technique, and post-processing parameters.

Kapton, a versatile polymer often used in aerospace applications due to its thermal stability and dielectric properties, is currently of interest as a resilient mechanical material for miniaturized autonomous robotics.[11] Integrating nanoscale oxide membranes on such a platform could enable ultra-lightweight sensing and energy conversion devices. However, Kapton and comparable polymer systems have drastically different physical properties than oxides. For example, Kapton has a glass transition temperature of ~360 °C, whereas YDZ has a melting temperature of over 2000 °C; similarly, the thermal expansion coefficient of Kapton is

* Address correspondence to kkerman@fas.harvard.edu.

Received for review August 22, 2013 and accepted November 20, 2013.

Published online November 20, 2013
10.1021/nn404401c

5 times larger than that of YDZ in the 25−300 °C range.[12] Creating a stable self-supported oxide membrane on a polymer platform with significantly different physical properties requires crystalline films with tunable internal stress. In this work, we present a low-temperature thin film processing technique that results in crystalline films and can be used to independently control the stress state. Ultra-light-weight membranes can subsequently be integrated as symbiotic "skins" on miniaturized robotic systems, functioning as power sources or sensors. We demonstrate integration of YDZ onto a Kapton support to form a functional thin film solid oxide fuel cell (TF-SOFC) operable below the polymer glass transition temperature. Our approach demonstrates new routes of integrating structural power sources on autonomous systems of growing interest in diverse engineering disciplines.

RESULTS AND DISCUSSION

Complexity in Fabrication of an Oxide Film onto a Polymer. Monolithic integration of brittle oxide membranes, such as YDZ, onto a polymer (Kapton in this study) requires significant experimental effort, briefly outlined in Figure 1. A thin polymer support is generally not suitable as a substrate on its own due to a lack of rigidity. As shown in Figure 1a, an as-grown YDZ film on bare Kapton creates a nonplanar structure, which leads to macroscopic cracks unsuitable for gas-tight, dense, and mechanically robust membrane structures. Substrate curling is a direct result of the internal stress of the oxide film, which will be discussed in detail below. To overcome this inherent difficulty, a polymer adhesive was used to bond Kapton onto a carbon fiber scaffold. This particular support was selected due to its mechanical resilience and current use as a structural material in the development of bioinspired insect-like robots.[11] The structure cannot be cleaned by traditional substrate methods (*i.e.*, organic solvent rinse and N_2 dry) as this may decompose the polymeric components or reduce the effectiveness of the adhesive. Therefore, we utilized an *in situ* Ar plasma treatment to remove adsorbed contaminants on the structure immediately preceding YDZ growth. Atomic force microscopy images of the bare Kapton surface before and after Ar plasma treatment indicated negligible surface morphology changes. Etching of Kapton to release the free-standing oxide membrane is recommended by DuPont using a mixture of potassium hydroxide, ethanol, and water. However, upon using this formulation, we encountered a severe reaction shown in Figure 1b. Therefore, a dry etching procedure was devised to remove the support without damaging the structure and maintaining the mechanical integrity of the YDZ membrane (see Experimental Methods). Based on the results of the study described herein, some representative successful examples of self-supported oxide nanomembranes on Kapton are shown in Figure 1d,e.

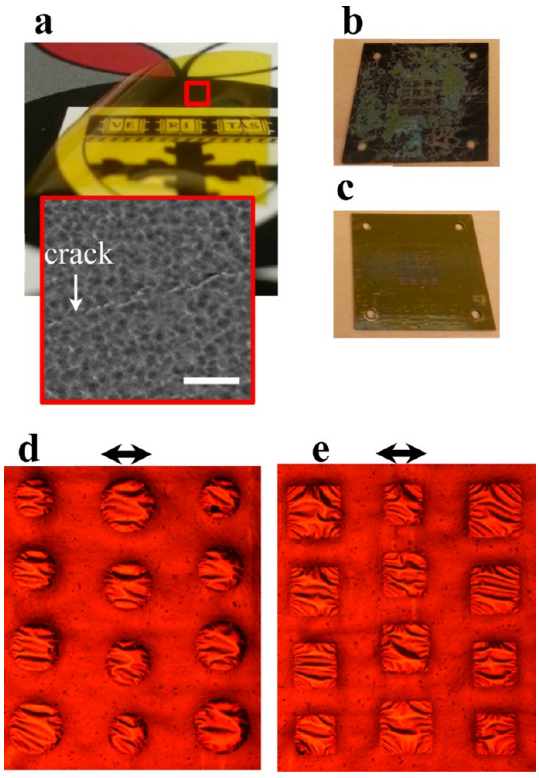

Figure 1. (a) Curling of a piece of Kapton after YDZ deposition with an inset showing a SEM image of YDZ microstructure showing a planar crack on the surface. The white scale bar is 200 nm; (b) 10 × 10 cm test structure of YDZ/Kapton/adhesive/carbon fiber depicting the catastrophic nature of wet etching and (c) successful dry etching protocol; (d) circular and (e) square YDZ membranes on a Kapton test structure after release. The arrow scales are 300 μm, the side length and diameter of the largest membranes made. Note that arbitrary membrane geometries are possible with this technique, whereas on Si different micromachining processes must be used to obtain alternative membrane geometry due to constraints of anisotropic wet etching.

Yttria-Doped Zirconia (YDZ) Film Characteristics. Films were grown at 550 or 30 °C by radio frequency sputtering from an 8 mol % YDZ target in an Ar environment. Details of film growth and characterization methods are provided in the Experimental Methods section. In order to fabricate a robust ultrathin membrane structure, crystalline films with controllable internal stress (σ_0) are necessary. This is to ensure that a structurally induced lattice distortion does not rupture the membrane,[3] and that the released structure will be elastically stable under self-supporting conditions.[13]

Internal Stress. Prior work on the effects of various parameters on sputtered film stress for elemental metal systems shows that the origin of σ_0 can be either extrinsic or intrinsic.[14,15] The former is thermally induced by virtue of substrate and film having different expansion coefficients, while the latter is either impurity or atomic peening induced.[15] Figure 2 summarizes the effect of deposition pressure (P) on σ_0 for a

constant YDZ film thickness of ~100 nm. Compressive stress indicates that the thermally induced extrinsic component is small, as one would expect a tensile contributed based on the differences in coefficient of thermal expansion between Si and YDZ. The small extrinsic component is also supported by the comparable σ_0 for films processed at 550 and 30 °C. For the latter, there is crossover in stress from compressive to tensile at $P \sim 0.55$ Pa. This is a result of the increasing scattering events at high pressure, leading to multidirectional velocity components of ions reaching the film surface.[15] Films grown at 550 °C appear to approach this crossover at a slightly higher deposition pressure, likely related to elevated surface temperature. The ability to produce a compressive internal stress in the oxide film is a desirable condition to fabricate robust self-supported membranes that do not rupture from tensile fracture upon external perturbations.

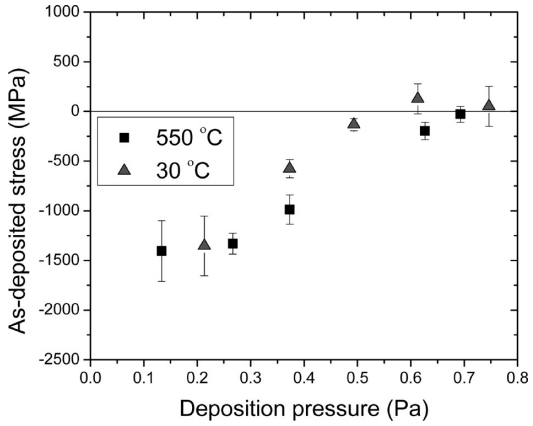

Figure 2. Internal stress measured by wafer curvature changes for YDZ films on Si_3N_4/Si substrates with error bars corresponding to ±3 standard deviations obtained from 12 measurements on each wafer.

Prior work on reactively sputtered YDZ reported deposition pressure dependence of internal stress for ~250 nm thick films.[16] We point out some key differences between our observations and that of ref 16. As previously shown,[13,16] the internal stress of YDZ is a function of thickness at constant pressure. Therefore, for a given thickness, the functional dependence of internal stress on deposition pressure may not necessarily be compared. In ref 16, there is a sharp crossover pressure at $P \sim 1.33$ Pa, and the lowest deposition pressure studied is $P \sim 0.66$ Pa. In our work, we demonstrate for the first time the ability to control the internal stress in the very narrow deposition pressure range of $0.13 < P < 0.7$ Pa. Finally, there are variations in reported values of internal stress for YDZ, likely due to the subtle differences of specific deposition conditions. This subtlety can be of extraordinary

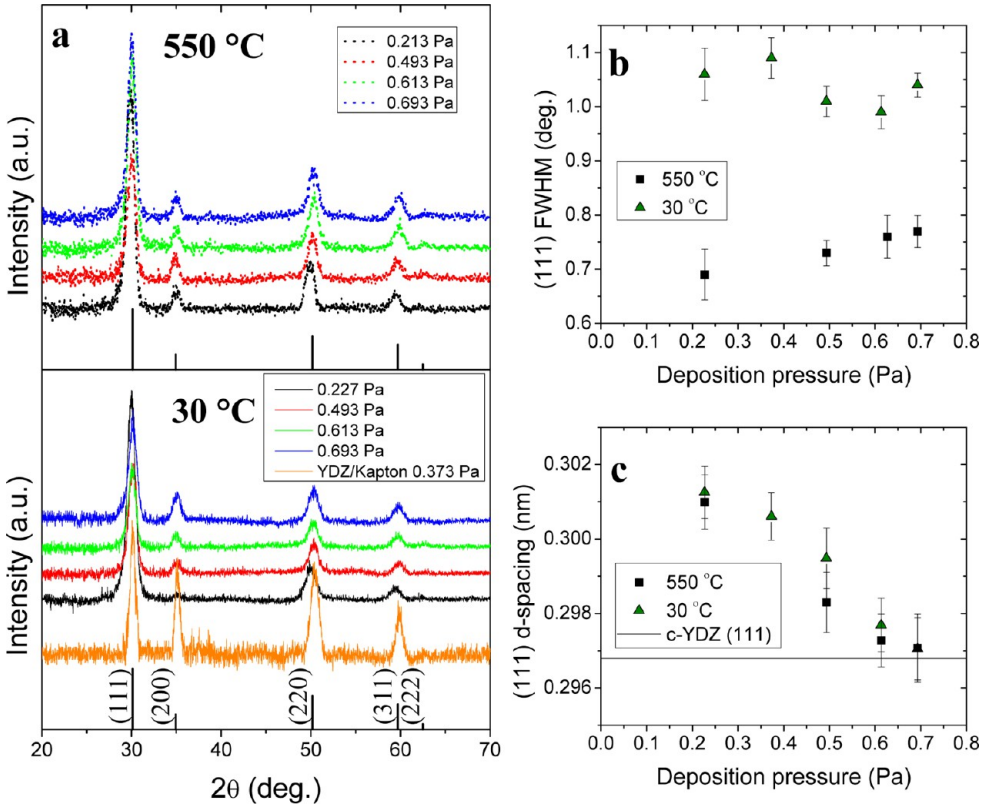

Figure 3. (a) GIXRD on as-grown films on Si_3N_4/Si indexed to cubic YDZ using ICDD 00-030-1468; (b) fwhm of (111) as a function of deposition pressure for YDZ films on Si_3N_4/Si substrates showing minute deposition pressure dependence within error limits; (c) (111) *d*-spacing with cubic YDZ referenced, verifying an accompanying local lattice distortion as a function of deposition pressure.

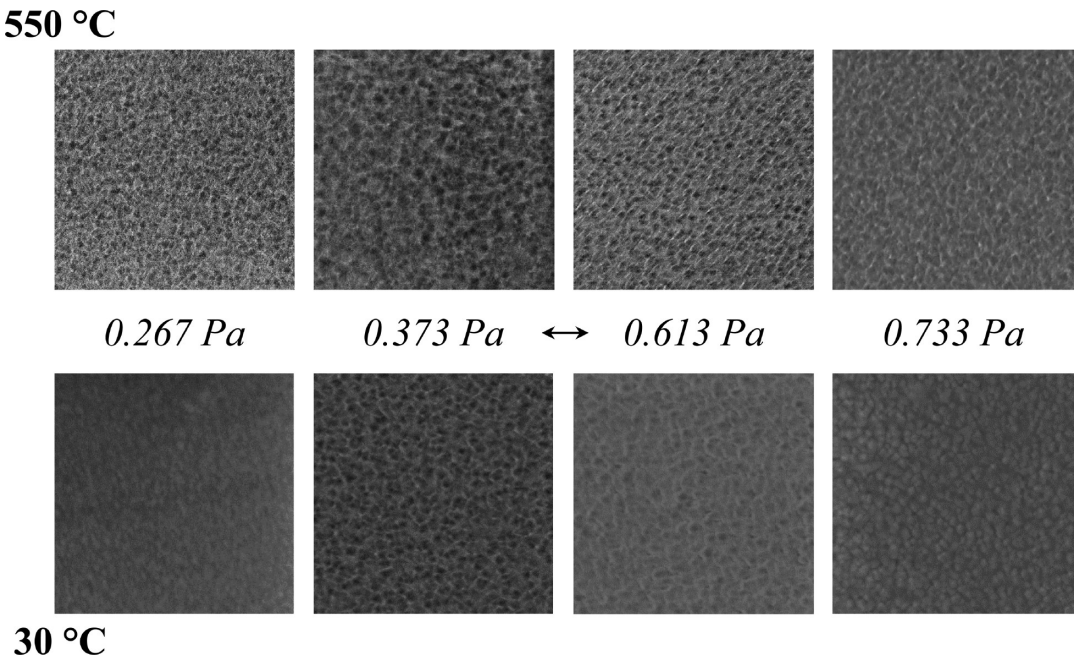

Figure 4. SEM micrographs of YDZ films grown on Si_3N_4/Si substrates at various pressures showing a similar nanogranular structure, independent of temperature. The central scale bar is 200 nm.

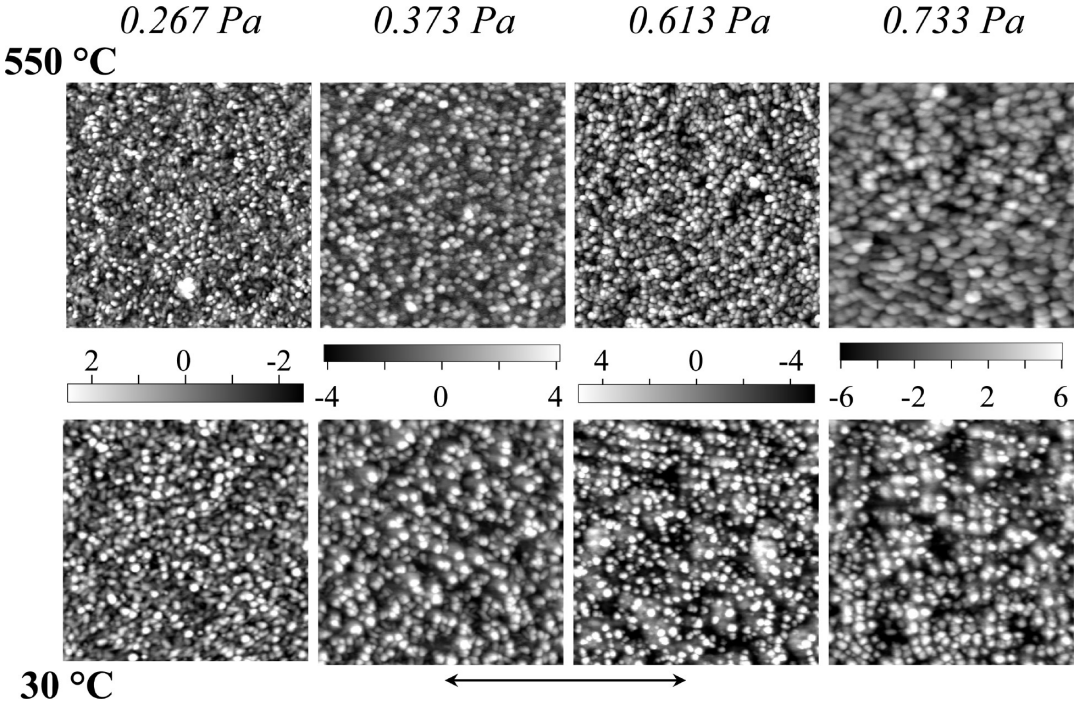

Figure 5. AFM images of YDZ films grown on Si_3N_4/Si substrates at various pressures showing similar microstructures. The AFM scale bar shows range in nanometers, while the central lateral scale is 1 μm, the side length of each scan.

importance when it comes to fabricating free-standing membrane structures since regions of elastic stability for buckled self-supported membranes are directly proportional to σ_0, which as we show here can be quite sensitive to deposition pressure, among other important parameters.[13,17]

Crystallinity and Phase. Figure 3 shows the physical characterization of films grown at 550 and 30 °C. Grazing incidence X-ray diffraction (GIXRD) patterns in Figure 3a indicate that all films are crystalline and can be indexed to a cubic phase. We do not observe any clear amorphous signatures in raw GIXRD patterns. As discussed above, the ability to grow crystalline oxide films with controllable stress is a crucial step that allows us to build devices with suspended membranes. Figure 3b plots the fwhm from (111) GIXRD peaks for

both sets of films showing similar results within error limits, indicating that crystallite size and possibly microstrain within grains are comparable. Figure 3c shows the out-of-plane (111) spacing, indicating an increase in out-of-plane spacing as deposition pressure is reduced, which implies a contracted in-plane lattice spacing confirming the increase of compressive biaxial internal stress. Variation of interplanar spacings for other orientations and additional discussion can be found in the Supporting Information.

Crystallinity of a YDZ film grown on Kapton is demonstrated in the bottom portion of Figure 3a, where GIXRD data appear similar to that of films grown on Si_3N_4/Si. Since GIXRD experiments were performed under congruent conditions, the slightly different behavior of the fwhm of YDZ films on Kapton may imply a larger grain size or smaller microstrain compared to YDZ on Si_3N_4/Si substrates, which are both discussed further in the following section and the Supporting Information, respectively.

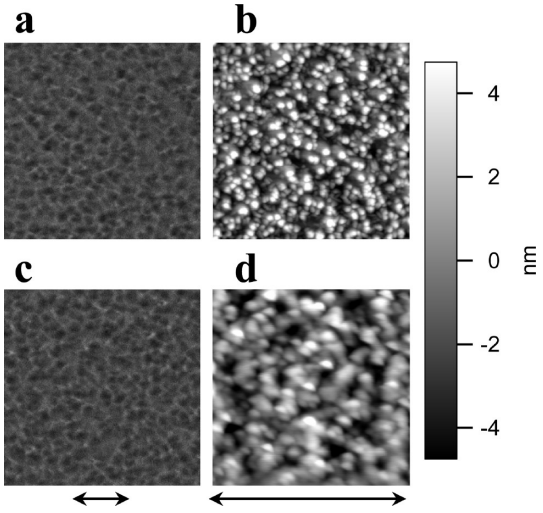

Figure 6. SEM and AFM images of YDZ films grown at 30 °C on Si_3N_4/Si (a,b) and Kapton (c,d) substrates at 0.373 Pa. AFM images highlight the larger grain size of YDZ on Kapton. The central scale below SEM images is 200 nm, while that below AFM images is 1 μm.

Microstructure. Scanning electron microscopy (SEM) and atomic force microscopy (AFM) were used to investigate the surface morphology and microstructure of YDZ films on Si_3N_4/Si and Kapton. Figure 4 and Figure 5 show SEM and AFM images of YDZ films grown

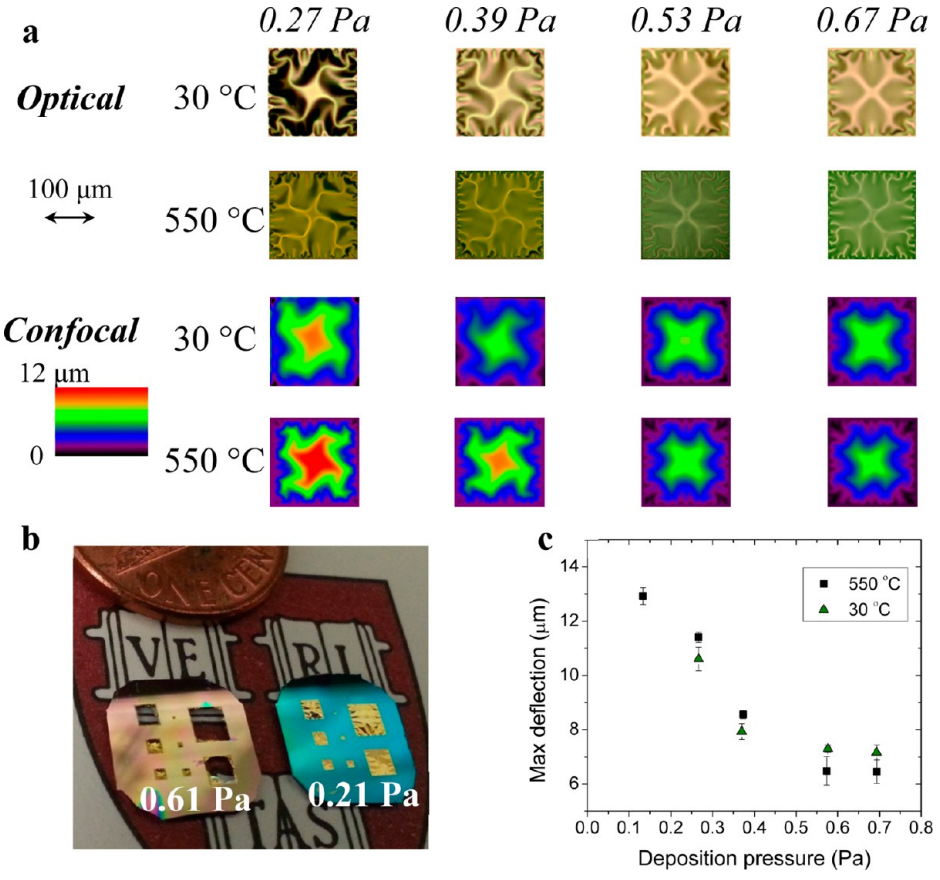

Figure 7. (a) Optical and confocal images of self-supported YDZ membranes having fixed L/h (160 μm/100 nm) and corresponding deposition pressures. The buckling patterns are consistent with previous work in a similar $\sigma \sim \sigma_0$ range.[15,18] Of note is that even samples grown at ~0.7 Pa are buckled though σ_0 is small. This is a result of controlling σ_0 independent of h, allowing L/h to remain large enough to observe buckled configurations. (b) Two test chips with self-supported YDZ films grown at 30 °C using different deposition pressure spanning side lengths of 0.15−2.5 mm, demonstrating stress-controlled scalability. (c) Maximum deflection of membranes shown in (a) as a function of deposition pressure as measured by confocal microscopy. A monotonic decrease in deflection of the buckled membranes corroborates the decrease in compressive stress with increasing pressure.

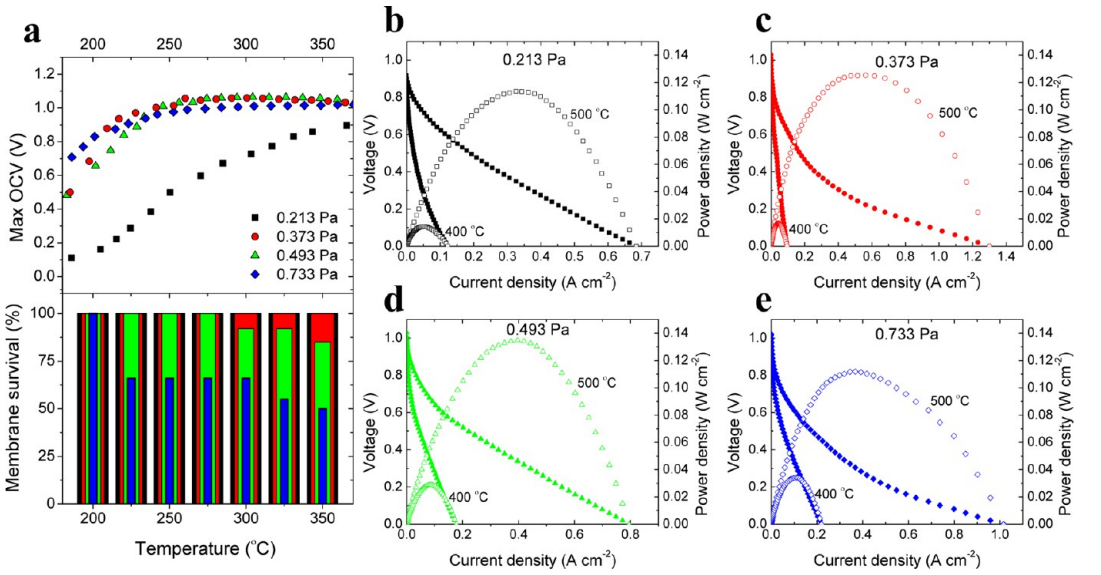

Figure 8. (a) OCV and membrane mechanical survival statistics (minimum of 18 samples) of TF-SOFCs fabricated on Si platforms for several deposition pressures, as a function of temperature. Current−voltage (closed symbols) and current−power (open symbols) curves are shown for TF-SOFCs using YDZ fabricated at varying deposition pressures; (b) 0.213 Pa, (c) 0.373 Pa, (d) 0.493 Pa, (e) 0.733 Pa.

on Si_3N_4/Si at varying deposition pressures. All films exhibited a granular texture having nanoscale grains and comparable microstructures. The surface roughness of YDZ films was found to monotonically increase with increasing deposition pressure. The dependence is shown in the Supporting Information; it appears independent of deposition temperature and nearly linear. Figure 6 exhibits the microstructure of YDZ films on Si_3N_4/Si and Kapton substrates grown at 30 °C and $P \sim 0.373$ Pa, indicating similar behavior. YDZ films on Kapton appear to show a larger average grain size based on AFM images, which supports the narrower fwhm observed in GIXRD.

YDZ Membrane Characteristics. Upon release from a substrate support, thin films form clamped membranes that buckle as a result of the internal stress in the released film. For high orders of buckling, that is, beyond a single buckled wavelength along boundary layers, the periodicity and amplitude of deformations along the clamped boundary are closely related to the internal stress. For buckled square membranes with small changes in the out-of-plane displacement, the scaled stress, $\sigma\sim_0 = (\sigma_0/E)(L/h)^2$, has been shown to accurately describe elastic configurations.[13] In this expression, E, L, and h represent elastic modulus, membrane side length, and film thickness, respectively. Stable configurations for a given set of boundary conditions, for example, fixed L, can be described by a range of $\sigma\sim_0$ values. During deposition, h can be controlled, however, as discussed previously, σ_0 is known to be a function of h in metals and YDZ.[13,16,18] Therefore, exclusive control of σ_0 is vital for forming robust nanoscale membranes for any L or h. Further, control of σ_0 independent of temperature enables the formation of stable membranes processed at low temperature and the ability to counteract any thermally generated stresses that may cause rupture as it is favorable for membranes to remain in a compressive regime throughout operation to prevent tensile stress induced failure. However, it should be noted that buckling induced by compressive internal stress inevitably causes tensile stresses along the periodic ripples. For square membranes having $L \sim 160$ μm, it has been shown that the maximum tensile stress generated from buckling is comparable to σ_0,[13] though care should be taken when considering nonlinear design of such membranes.[8] We fabricated self-supported YDZ membranes on Si platforms at constant L/h (160 μm/100 nm) grown at various deposition pressures.

YDZ Membrane Buckling. Confocal and optical micrographs of the membranes as a function of deposition pressure are presented in Figure 7. The buckling configurations are strikingly similar for both deposition temperatures, confirming the ability to independently control stress and form stable membrane structures for a given aspect ratio at temperatures as low as 30 °C. Interestingly, even in the case when $|\sigma_0|$ is small, stable buckling configurations are observed. This is a key result of this study that allows the realization of suspended membranes on Kapton since scaling σ_0 using h at constant pressure requires unreasonable thicknesses or leads to unstable flat membranes.[13,17] Figure 7b exhibits the utility of this process by comparing two samples grown at low temperature and different pressure having eight different side lengths, hence changing L/h at constant h, and independently controlling σ_0. As shown, if σ_0 is adequately compressive,

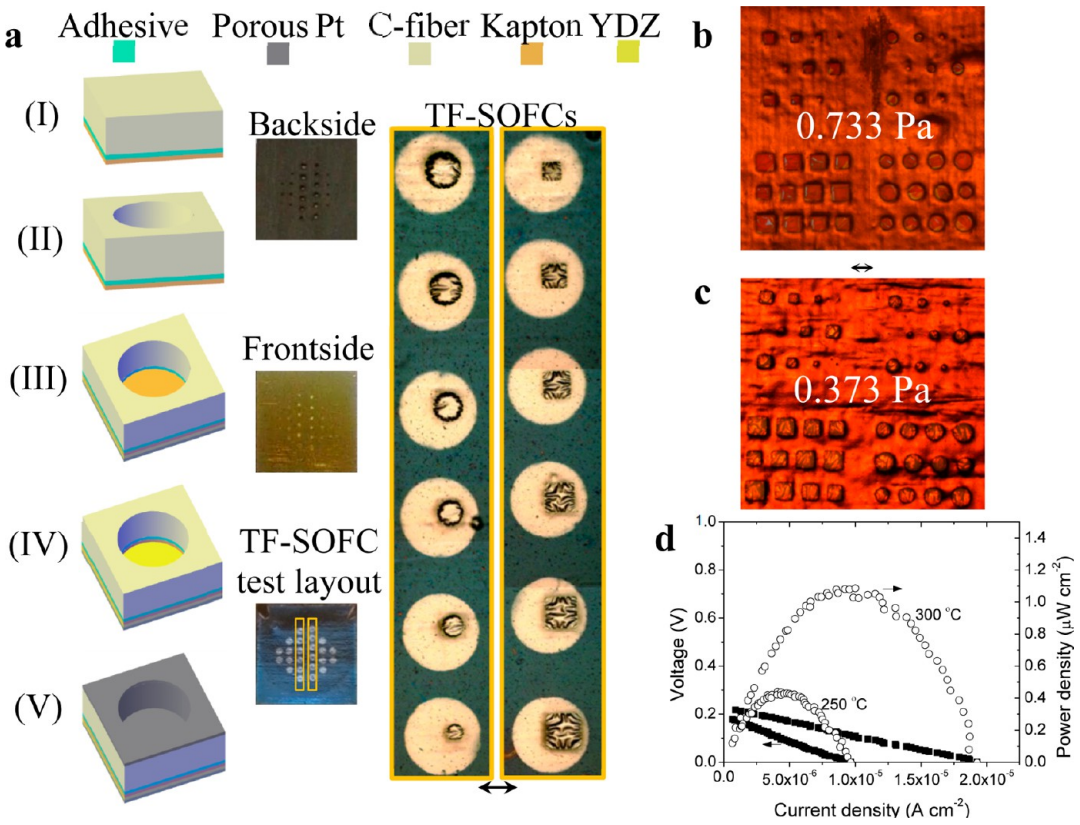

Figure 9. (a) Schematic process flow for integrating YDZ grown at 30 °C onto bioinspired Kapton structures and forming a self-supported membrane with optical micrographs. The processing steps are as follows: (I) bonding of Kapton onto a structural robotic carbon fiber composite; (II) laser cutting of carbon fiber to expose backside of Kapton; (III) deposition of crystalline YDZ at 30 °C on the frontside followed by porous Pt; (IV) dry etching of the backside to release the bilayer Pt/YDZ membrane from Kapton support; and (V) deposition of porous Pt on the backside to complete the self-supported trilayer heterostructure. Final TF-SOFC heterostructures (Pt/YDZ/Pt) are shown in the optical micrograph having side length/diameters in the 0.15−0.3 mm range. Optical images of thermally cycled (25−300 °C) YDZ membranes grown at different pressures on Kapton scaffolds are shown in (b), where all membranes are broken and (c) where all membranes have survived. The YDZ membranes range from 0.05 to 0.3 mm in side length/diameter. Both scale bars shown represent 300 μm in length. (d) Current−voltage and current−power plot for a representative TF-SOFC on Kapton having a radius of 0.1 mm with self-supported YDZ electrolytes grown at 30 °C, exhibiting the ability to integrate low-temperature membranes into a working device.

scalable self-supported YDZ membranes grown at 30 °C can be fabricated without any additional support layers. Figure 7c shows out-of-plane deflection data for the membranes, which can potentially be used for calculating local stress on the membrane and possibly predicting failure. Although values of σ_0 for YDZ films on Kapton may not be exactly the same as YDZ grown on Si_3N_4/Si control samples, the functional dependence on deposition pressure likely remains. As shown in Figure 1, this information enables the ability to integrate stable oxide membranes onto a polymer scaffold, much like a lightweight skin.

Thermomechanical Stability and Fuel Cells. TF-SOFCs were fabricated on Si platforms with symmetric Pt electrodes to evaluate the role of deposition pressure on electrochemical characteristics. Figure 8a shows the maximum open circuit voltage (OCV) and membrane mechanical survival statistics obtained for several deposition pressures as a function of temperature. With the exception of the $P = 0.213$ Pa sample set, the YDZ membranes appear to exhibit a nearly perfect OCV. The behavior of the lowest pressure set may be related to its large membrane deformations which could lead to a network of noncritical cracks for mechanical integrity but leading to reduction in the open circuit voltage. The survivability of the nanoscale membranes is also temperature- and *P*-dependent. Only samples with adequately compressive σ_0 can counteract the additional thermal stress imparted during heating and cooling under an electric load. Representative current−voltage and current−power curves for these TF-SOFCs are shown in Figure 8b−e. The maximum power density appears independent of deposition pressure and is ~125 mW cm^{-2} at 500 °C. This is lower than what has been previously reported in the TF-SOFC literature; however, it has been clearly shown that the nanoporous metallic electrode microstructure plays a profound role in a wide range of TF-SOFC performances reported.[19] We do not explore optimization

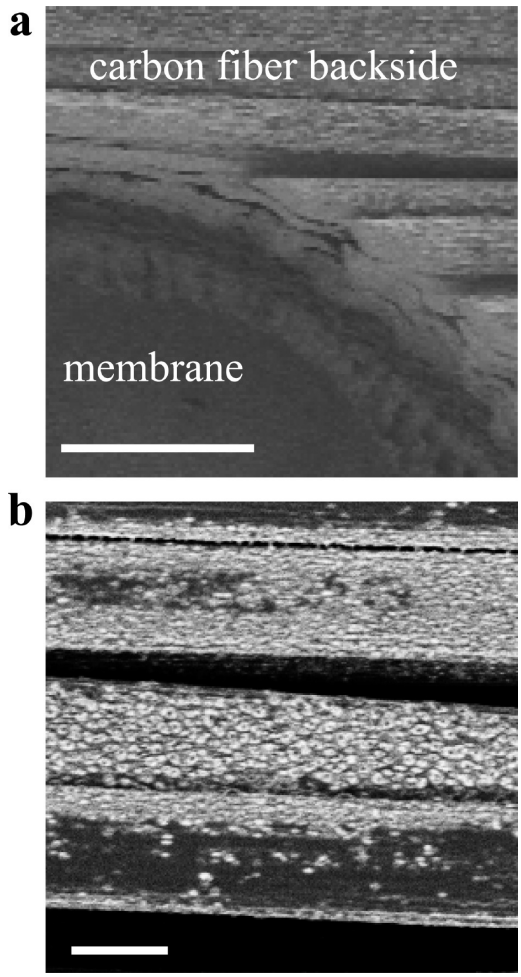

Figure 10. (a) SEM image of the backside of a fabricated YDZ/Kapton/carbon fiber structure showing the side wall profile of the carbon fiber scaffold from laser cutting. The scale bar is 20 μm. (b) Image showing the lack of connectivity of Pt on carbon fiber supports after fuel cell testing. The scale bar is 5 μm.

conditions in this study and only note that electrodes for all samples were grown concurrently, ensuring a systematic comparison.

YDZ Membrane Integration onto Kapton. With knowledge of the mechanical, material, and electrochemical implications of deposition pressure, we integrated YDZ membranes on Kapton through the procedure outlined in Figure 9a. Optical micrographs in Figure 1 and Figure 9b,c illustrate the scalability of nanoscale membranes formed directly on Kapton scaffolds. As shown in Figure 9c, proper control of the internal stress in YDZ allows the membranes to be stable and survive thermal cycling from 25 to 300 °C. As a proof of concept, TF-SOFC devices were fabricated in a similar fashion to Si platforms utilizing symmetric Pt electrodes. Figure 9d shows the current–voltage and current–power behavior of a representative device at several temperatures. The maximum OCV is ~220 mV, which deviates from the ideal value of ~1 V under these testing conditions, possibly indicating electronic leakage or minute defects in the membranes as discussed above for the P = 0.213 Pa sample set on Si_3N_4/Si. We note that the OCV and power density of these devices are lower than what has previously been achieved on Si or glass.[4,5,19] While this could be due to many factors, it is partially attributed to the overall complexity in the support scaffold. As shown in Figure 10a, the backside of the structure is far from ideal. The laser cut side walls of the carbon fiber scaffold make deposition of high-performance electrodes on the structure challenging. This is shown in more detail in the SEM image of the Pt electrodes after TF-SOFC operation on the carbon fibers in Figure 10b; optimizing this aspect would be the subject of a future study. The main feature of this work is establishing independent control of internal stress in a crystalline oxygen-ion conducting film grown at 30 °C, directly enabling the fabrication of robust nanoscale membranes, which leads to the demonstration of a structurally integrated power source having potential application as an energy conversion or sensing element for miniature autonomous robotic systems.

CONCLUSIONS

We have presented a general processing route in which the internal stress of an archetypal crystalline oxygen-ion conductor can be controlled over a narrow pressure range independent of temperature. Utilizing this degree of freedom, we have fabricated self-supported oxide membranes that are thermomechanically stable. Low-temperature, stress-controlled growth of thin films has enabled the capability of integrating a brittle oxide membrane onto a widely used polymer scaffold currently of interest as a structural component for robotic systems. We demonstrated that this membrane can function as a thin film solid oxide fuel cell operating below the glass transition of the polymer, thereby creating a monolithically integrated structural power generation device. The results may be of relevance toward future integration of on-board power systems, requiring monolithic combination of materials with vastly different physical properties.

EXPERIMENTAL METHODS

All films were grown by radio frequency magnetron sputtering (AJA International) from a 2 in. diameter, 8 mol % YDZ target (Plasmaterials Inc.) at 100 W in an Ar environment. Growth pressure was controlled using an adaptive pressure regulator controlling a throttle valve. Growth rate was approximately constant with pressure. The growth temperature for films grown without substrate heating was estimated by using an interferometer during growth and verified by placing a thermocouple on the substrate holder immediately after (less than 5 min) growth. Internal stress in the films was determined by measuring wafer curvature changes (Toho FLX-2320-S) and using

Stoney's equation[20]

$$\sigma_0 = \frac{E_S}{1-\nu_S}\frac{\Delta K}{6}\frac{h_S^2}{h_f}$$

where $E_S/(1-\nu_S)$, ΔK, h_S, and h_f are the substrate biaxial modulus, change in curvature, substrate thickness, and film thickness, respectively. Film thickness and growth rate were obtained by low angle reflectivity using a coupled scan in the $0.4 < 2\theta < 3$ range using a step size of 0.002° with parallel beam optics (Bruker D8, Cu anode). Phase information was gathered by fixing $\Omega = 1°$ and scanning from $20° < 2\theta < 70°$ with a step size of 0.01°. Surface morphology and roughness for samples on Si_3N_4/Si were measured in tapping mode (Asylum) using Al/Si cantilevers (Asylum AC160TS). YDZ samples on Kapton were imaged in contact mode, with Al/Si cantilevers (Pointprobe FMR-10). Images of film surfaces were taken (Zeiss Ultra-Plus) using a charge-compensating electric charge dissipater and the in-lens detector at an accelerating voltage of 3 kV. Out-of-plane deflection was determined using a laser confocal microscope (Olympus LEXT OLS4000). Microfabrication methods were used to photolithographically pattern and etch a Si_3N_4/Si wafer. KOH (30 wt %) was used to etch Si, while a mixture of CF_4 and O_2 (15/12) was used to etch Si_3N_4. Nanoporous Pt for fuel cell testing was deposited by DC sputtering at 250 W in 75 mTorr of Ar without substrate heating. Kapton (180 μm) was bonded to custom-made carbon fiber composites using an acrylic adhesive (Pyralux by DuPont). The structure was then laser cut to an assembly of self-supported Kapton. After YDZ growth, this support was etched in a mixture of CF_4 and O_2 (30/100) to form self-supported YDZ. A custom-built two-chamber test system with a gold ring seal was used to test the fuel cells. Standing laboratory air was the oxidant, and humidified 5% H_2 in an Ar carrier gas was used as fuel, which was fed at a rate of 30 sccm/min.

Conflict of Interest: The authors declare no competing financial interest.

Acknowledgment. This work was supported by NSF Grant No. CCF-0926148. K.K. was supported by the Department of Defense through the National Defense Science & Engineering Graduate Fellowship (NDSEG) Program. Q.V.O. acknowledges financial support from the F.R.S.-FNRS through a postdoctoral scholarship.

Supporting Information Available: Additional discussion on stress, sample preparation, and film characterization. This material is available free of charge *via* the Internet at http://pubs.acs.org.

REFERENCES AND NOTES

1. Kim, M.-G.; Kanatzidis, M. G.; Facchetti, A.; Marks, T. J. Low-Temperature Fabrication of High-Performance Metal Oxide Thin-Film Electronics *via* Combustion Processing. *Nat. Mater.* **2011**, *10*, 382–388.
2. Banger, K. K.; Yamashita, Y.; Mori, K.; Peterson, R. L.; Leedham, T.; Rickard, J.; Sirringhaus, H. Low-Temperature, High-Performance Solution-Processed Metal Oxide Thin-Film Transistors Formed by a 'Sol–Gel on Chip' Process. *Nat. Mater.* **2011**, *10*, 45–50.
3. Balakrishnan, V.; Ko, C.; Ramanathan, S. *In Situ* Studies on Twinning and Cracking Proximal to Insulator–Metal Transition in Self-Supported VO_2/Si_3N_4 Membranes. *J. Mater. Res.* **2012**, *27*, 1476–1481.
4. Chao, C. C.; Hsu, C. M.; Cui, Y.; Prinz, F. B. Improved Solid Oxide Fuel Cell Performance with Nanostructured Electrolytes. *ACS Nano* **2011**, *5*, 5692–5696.
5. Muecke, U. P.; Beckel, D.; Bernard, A.; Bieberle-Hütter, A.; Graf, S.; Infortuna, A.; Müller, P.; Rupp, J. L. M.; Schneider, J.; Gauckler, L. J. Micro Solid Oxide Fuel Cells on Glass Ceramic Substrates. *Adv. Funct. Mater.* **2008**, *18*, 3158–3168.
6. Baker, R. W. Future Directions of Membrane Gas Separation Technology. *Ind. Eng. Chem. Res.* **2002**, *41*, 1393–1411.
7. Lubomirsky, I. Stress Adaptation in Ceramic Thin Films. *Phys. Chem. Chem. Phys.* **2007**, *9*, 3701–3710.
8. Yamamoto, N.; Quinn, D. J.; Wicks, N.; Hertz, J. L.; Cui, J.; Tuller, H. L.; Wardle, B. L. Nonlinear Thermomechanical Design of Microfabricated Thin Plate Devices in the Post-buckling Regime. *J. Micromech. Microeng.* **2010**, *20*, 035027.
9. Ziebart, V.; Paul, O.; Baltes, H. Strongly Buckled Square Micromachined Membranes. *J. Microelectromech. Syst.* **1999**, *8*, 423–432.
10. Baertsch, C. D.; Jensen, K. F.; Hertz, J. L.; Tuller, H. L.; Vengallatore, S. T.; Spearing, S. M.; Schmidt, M. A. Fabrication and Structural Characterization of Self-Supporting Electrolyte Membranes for a Micro Solid-Oxide Fuel Cell. *J. Mater. Res.* **2004**, *19*, 2604–2615.
11. Wood, R.; Finio, B.; Karpelson, M.; Ma, K.; Pérez-Arancibia, N.; Sreetharan, P.; Tanaka, H.; Whitney, J. Progress on 'Pico' Air Vehicles. *Int. J. Robot Res.* **2012**, *31*, 1292–1302.
12. DuPont Kapton Technical Data Sheet. http://www2.dupont.com/Kapton/en_US/assets/downloads/pdf/HN_datasheet.pdf (accessed June 5, 2013).
13. Kerman, K.; Tallinen, T.; Ramanathan, S.; Mahadevan, L. Elastic Configurations of Self-Supported Membranes for Fuel Cells. *J. Power Sources* **2013**, *222*, 359–366.
14. Thornton, J. A.; Hoffman, D. W. Stress Related Effects in Thin Films. *Thin Solid Films* **1989**, *171*, 5–31.
15. Windischmann, H. Intrinsic Stress in Sputter-Deposited Thin Films. *Crit. Rev. Solid State Mater. Sci.* **1992**, *17*, 547–596.
16. Quinn, D. J.; Wardle, B.; Spearing, S. M. Residual Stress and Microstructure of As-Deposited and Annealed, Sputtered Yttria-Stabilized Zirconia Thin Films. *J. Mater. Res.* **2008**, *23*, 609–618.
17. Evans, A.; Prestat, M.; Tolke, R.; Schlupp, M. V. P.; Gauckler, L. J.; Safa, Y.; Hocker, T.; Courbat, J.; Briand, D.; de Rooij, N. F.; *et al.* Residual Stress and Buckling Patterns of Free-Standing Yttria-Stabilized-Zirconia Membranes Fabricated by Pulsed Lased Deposition. *Fuel Cells* **2012**, *12*, 614–623.
18. Spaepen, F. Interfaces and Stresses in Thin Films. *Acta Mater.* **2000**, *48*, 31–42.
19. Kerman, K.; Lai, B. K.; Ramanathan, S. $Pt/Y_{0.16}Zr_{0.84}O_{1.92}$/Pt Thin Film Solid Oxide Fuel Cells: Electrode Microstructure and Stability Considerations. *J. Power Sources* **2011**, *196*, 2608–2614.
20. Stoney, G. G. The Tension of Metallic Films Deposited by Electrolysis. *Proc. R. Soc. London, Ser. A* **1909**, *82*, 172–175.